JAEA-Data/Code
2018-007
DOI:10.11484/jaea-data-code-2018-007

JAEA-Data/Code

Geant4 Physics Process for Elastic Scattering of γ-Rays

Mohamed OMER and Ryoichi HAJIMA

Integrated Support Center for Nuclear Nonproliferation and Nuclear Security

June 2018

Japan Atomic Energy Agency

日本原子力研究開発機構

本レポートは国立研究開発法人日本原子力研究開発機構が不定期に発行する成果報告書です。
本レポートの入手並びに著作権利用に関するお問い合わせは、下記あてにお問い合わせ下さい。
なお、本レポートの全文は日本原子力研究開発機構ホームページ（http://www.jaea.go.jp）
より発信されています。

国立研究開発法人日本原子力研究開発機構 研究連携成果展開部 研究成果管理課
〒319-1195 茨城県那珂郡東海村大字白方 2 番地4
電話 029-282-6387, Fax 029-282-5920, E-mail:ird-support@jaea.go.jp

This report is issued irregularly by Japan Atomic Energy Agency.
Inquiries about availability and/or copyright of this report should be addressed to
Institutional Repository Section,
Intellectual Resources Management and R&D Collaboration Department,
Japan Atomic Energy Agency.
2-4 Shirakata, Tokai-mura, Naka-gun, Ibaraki-ken 319-1195 Japan
Tel +81-29-282-6387, Fax +81-29-282-5920, E-mail:ird-support@jaea.go.jp

JAEA-Data/Code 2018-007

Geant4 Physics Process for Elastic Scattering of γ-Rays

Mohamed OMER※ and Ryoichi HAJIMA*

Integrated Support Center for Nuclear Nonproliferation and Nuclear Security,
Japan Atomic Energy Agency
Tokai-mura, Naka-gun, Ibaraki-ken

(Received April 16, 2018)

Although the elastic scattering of γ-rays is already treated in many Monte Carlo simulation codes including Geant4, the representation of such simulations is still unsatisfactory in terms of the ability of the simulation to reproduce the experimental observations. Such inconsistency with experimental data is attributed to the fact that all current simulations implement Rayleigh scattering as the unique contributor to the total elastic scattering, ignoring other significant processes such as Delbrück scattering.

In this work, we describe a Geant4 simulation code that takes all contributing processes to the elastic scattering of γ-rays into consideration and emphasizes the possible interference between the different scattering amplitudes of different processes. The simulation covers all elements with the whole angular domain and over few MeV energy range.

Keywords: Elastic Scattering, γ-Rays, Rayleigh Scattering, Delbrück Scattering, Geant4

※ Senior Post-Doctoral Fellow

* National Institutes for Quantum and Radiological Science and Technology

JAEA-Data/Code 2018-007

ガンマ線の弾性散乱の Geant4 物理プロセス

日本原子力研究開発機構　核不拡散・核セキュリティ総合支援センター
Mohamed OMER※、羽島 良一*

(2018 年 4 月 16 日　受理)

Geant4 を含む多くのモンテカルロシミュレーションコードでは、ガンマ線（高エネルギー光子）の弾性散乱はすでに実装されているが、これらシミュレーションの実装は、実験結果を再現するだけの十分な精度を有していない。このような実験データとの不一致は、これまでのシミュレーションコードが弾性散乱としてレイリー散乱のみを考慮し、デルブリュック散乱などの他の重要なプロセスを無視していることに起因している。

本報では、弾性散乱に寄与するすべてのプロセスを考慮し、新たに整備した異なるプロセスの散乱振幅間の干渉効果を含んだ Geant4 シミュレーションコードについて述べる。 このシミュレーションコードは、全ての散乱角度領域および数 MeV エネルギー範囲にわたって、すべての元素を対象にした弾性散乱を取り扱うことができる。

原子力科学研究所：〒319-1195　茨城県那珂郡東海村大字白方 2-4
※ 任期付研究員
* 量子科学技術研究開発機構

Contents

目　次

Tables List

Figures List

1. Introduction

This report describes a simulation code for the elastic scattering of γ-rays based on the Geant4 simulation kit [1]. The research is a part of the ongoing R&D at the Japan Atomic Energy Agency (JAEA) since 2015 and is devoted to developing technologies for the nondestructive assay (NDA) of nuclear materials using the nuclear resonance fluorescence (NRF). The current report provides detailed illustrations on the γ-rays elastic scattering simulation code which has recently been published [2].

1.1 Interactions of γ-rays with materials

Several interactions of γ-rays with materials have, for different extents, effects on the NDA of materials. For the nuclear materials, whose NRF levels lie in the 2~3 MeV region, many interactions such as photoelectric effect, Compton scattering, pair production, and elastic (coherent) scattering have considerable cross sections in this range of γ-ray energies. As a result, they interfere the NRF detection as a background radiation. Therefore, this section is aimed at reviewing the different interactions that γ-ray may have with the materials at the anticipated energy range.

In general, the interaction of γ-ray photons with materials can be classified into two major categories. First is the absorption of the γ-ray photon within the material. This process includes the transmission as well because the transmitted intensity of a photon beam can be expressed as a complement of the absorbed intensity. The second category is the scattering of the γ-ray photon by the microscopic constitutes of the material whether they are atomic electrons, nuclei, or the electric fields surrounding them. Indeed, the scattering itself is sub-classified into two categories, elastic and inelastic scattering. For each category, there are some interactions may be possible with different probabilities depending on the energy of the electromagnetic wave and the material properties. It should be noted that interactions taking place at higher energies including the ejection of sub-nuclear spices or nuclear fission are beyond the scope of the current work.

The possible interactions of γ-ray with microscopic constitutes of materials are listed below,

i. Interaction with the atomic electrons.
ii. Interaction with the atomic nucleus.
iii. Interaction with the electric fields of the atomic electrons or nuclei.

By combining the three interactions with the three categories, giving the process of either absorption the symbol A, elastic scattering the symbol ES and inelastic scattering

the symbol IS, there are 12 mechanisms that γ-ray can interact with materials. Of these 12 mechanisms [3-5], the most important are listed in Table 1. In the following, we provide some details about these relevant interactions. The atomic interactions, which represent the base of the γ-ray detection, are also given as well as the implications of each interaction on a NRF measurement.

1.1.1 Photoelectric absorption

When an incident photon having an energy of $h\nu$ collides with a bound electron (usually in the K or L shell), the energy of the photon is transferred to the atom and the electron is ejected from the atom with energy E_{PE} given by equation (1). The ejected electron is called a photoelectron. The photoelectric interaction is shown in Fig. 1. The momentum is conserved by the recoil of the entire residual atom. Since the energy of the incident γ-ray is likely higher than the binding energy of the electron E_B, the majority of the emitted photo-electors are from the K shell.

$$h\nu = E_B + E_{PE} \tag{1}$$

Characteristic X-ray and Auger electrons from the filling of the vacancy in the inner shell are observed. In a NRF experiment, the photoelectric effect contributes the background at very low energy, which does matter because of the high count rates that are involved by this interaction, especially if the energy is below 1 MeV. However, this very low energy can be suppressed by mounting a thin layer of copper or lead, so-called absorber, on the face of the detector.

The experimental data and some models [3] show that the cross section is directly proportional to Z^4 and inverse proportional to $(h\nu)^3$. Therefore, the cross section of the photoelectric effect may be roughly given by,

Table 1: The effective interactions of γ-ray with materials at 2~3 MeV.

Mechanism	Interaction	Phenomenon
A-i	Absorption of γ-rays by electrons	Photoelectric effect
A-ii	Absorption of γ-rays by nuclei	Nuclear photoelectric effect
A-iii	Absorption of γ-rays by the electric field	Pair production
ES-i	Elastic scattering of γ-rays by electrons	Rayleigh scattering
ES-ii	Elastic scattering of γ-rays by nuclei	Nuclear Thomson scattering
ES-iii	Elastic scattering of γ-rays the Coulomb field around nuclei	Delbrück scattering
IS-i	Inelastic scattering of γ-rays by electrons	Compton scattering
IS-ii	Inelastic scattering of γ-rays by nuclei	Nuclear Compton scattering

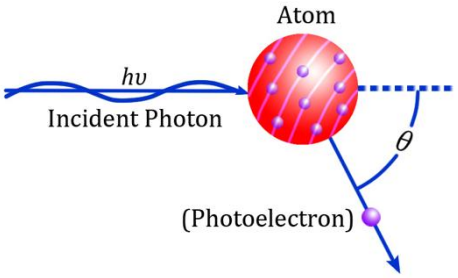

Fig. 1: Schematic diagram showing the photoelectric effect.

$$\sigma_{PE} \approx cons.\frac{Z^4}{E_\gamma^3} \tag{2}$$

The angular distribution of the ejected photoelectrons is most likely concentrated in the forward directions at energies more than 50 keV. Above 1 MeV, most of the photoelectrons are ejected not farther than 20° with respect to the incident γ-ray. The photoelectric effect is responsible for the γ-ray detection process. It mainly produces the photo-peak in γ-ray spectra measured within detectors. At very high energies of γ-ray (>100 MeV) where the cross section of the photoelectric effect vanishes and the photo-peaks are no longer observed with the γ-ray detectors.

1.1.2 Compton scattering

Unlike the photoelectric effect, Compton scattering is the process in which the incident photon transfers only a part of its energy to an atomic electron and therefore the photon is scattered with a lower energy. The difference in energies is transferred to the electron. Fig. 2 shows a schematic diagram of Compton scattering. Compton scattering (or incoherent scattering) is predominant in the 1~5 MeV energy range. That means, the binding energy of the electron is negligible relative to the incident photon energy. Thus, Compton scattering is usually considered as a collision between the incident photon and a free electron being initially at rest. In Compton scattering, the energy and momentum are conserved. As a result, the energy of the scattered photon can be easily formalized. The frequency of the scattered photon, ν', is related to the frequency of the incident photon, ν_o, by,

$$\frac{\nu'}{\nu_o} = \frac{1}{1+\alpha(1-cos\theta)}, \alpha = \frac{h\nu_o}{mc^2} \tag{3}$$

where θ is the scattering angle of the scattered photon. As noted from equation (3), in the backscattering case $(\theta = \pi)$ the scattered photon has the minimum energy.

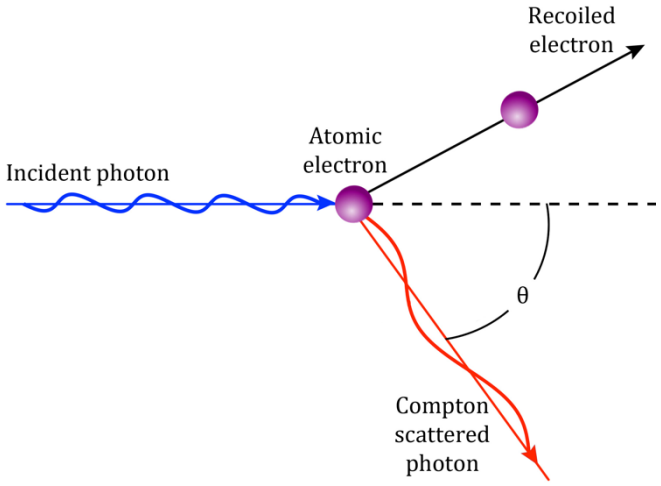

Fig. 2: Compton scattering.

On the other hand, forward scattering involves scattering of photons whose energies are not lowered so much. Therefore, like photoelectric effect, it is preferable to position the detector for a NRF measurement far from the incident beam direction because in this case the detector will only accept lower energy photons. However, the Compton scattered photons from a NRF target represents, as shown below, a huge background from the count rate prospective.

Compton scattering process provides absorption of a part of the incident beam energy and also scattering of the other part. So, when dealing with the Compton scattering cross section, firstly, the collision cross section is divided into two parts. One part for the absorbed energy and the complement is for the scattered energy. The collision differential cross section per electron, $d\sigma_C^c/d\,\Omega$, is number of scattered photons divided by the number of incident photons. This can be given by the Klein-Nishina formula [6,7],

$$\frac{d\sigma_C^c}{d\,\Omega} = \frac{r_o^2}{2}\left(\frac{\nu'}{\nu_o}\right)^2\left(\frac{\nu_o}{\nu'} + \frac{\nu'}{\nu_o} - sin^2\theta\right) \tag{4}$$

where $r_o = 2.818 \times 10^{-15}$ m is the classical electron radius. Integration of equation (4) for a given incident photon energy gives the total Compton scattering events per electron occurring within the target. It should be noted that equation (4) is for unpolarized photons and it can be given in terms of the incident photon energy by combining equations (3) and (4),

$$\frac{d\sigma_C^c}{d\,\Omega} = \frac{r_o^2}{2}\left(\frac{1}{1+\alpha(1-cos\theta)}\right)^2(1+cos^2\theta)\left(1+\frac{\alpha^2(1-cos\theta)^2}{(1+cos^2\theta)(1+(1-cos\theta))}\right) \tag{5}$$

The scattering differential cross section, $d\sigma_C^S/d\Omega$, is defined as the scattered energy per second divided by the incident intensity [6].

$$\frac{d\sigma_C^S}{d\Omega} = \frac{d\sigma_C^C}{d\Omega}\left(\frac{\nu'}{\nu_o}\right) = \frac{r_o^2}{2}\left(\frac{\nu'}{\nu_o}\right)^3\left(\frac{\nu'}{\nu_o} + \frac{\nu_o}{\nu'} - sin^2\theta\right) \quad (6)$$

It worth emphasizing that Compton scattering photons from a scatterer can be used as a means to measure the absolute flux of a γ-ray beam.

From the target prospective, Compton scattering represent the basic process in the attenuation of the γ-ray by the material. The attenuation includes the absorption of a part of the incident energy and the scattering another part. The intensity of the energy deposited in the material or the scattered by Compton scattering is directly proportional to the areal density of the scattering material. Therefore, the attenuation of a γ-ray beam by Compton scattering increases in case of heavy Z materials. Indeed, this represents a problem for the NDA of the nuclear materials since all of them are heavy elements. Overcoming the attenuation of γ-ray beam by the heavy materials requires much higher fluxes than currently available.

The angular distribution of the Compton scattered photons indicates that the scattered photons are likely scattered at small angle. Of course, it strongly depends on the energy of the incident photons. As an example, at 2 MeV the collision cross section drops from about 33 mb at 30° to about 4.7 mb at 150°. Therefore, in a NRF measurement, the detector should be positioned at backward directions to decrease the background coming from the Compton scattered photons by the target. The backward position of the detectors accepts lower number of the Compton scattered photons and hence the detector operates at lower count rates.

1.1.3 Pair production

When the incident photon has an energy of ≥ 1.02 MeV the photon may disappear in the proximity of the nucleus and an electron-positron pair is produced. The condition for this process is that the energy of the incident photon must exceed the rest energy of the electron-positron pair, *i.e.* 511 + 511 = 1022 keV. If the photon has energy higher than 1.02 MeV, the excess energy is transferred to kinetic energy of the electron and positron. Figure 3 shows a schematic diagram of the pair production process. Because the positron has a short lifetime, it combines with an electron in the absorbing material and they disappear giving up two oppositely directed γ-ray photons each has an energy of 511 keV. This process is called annihilation process.

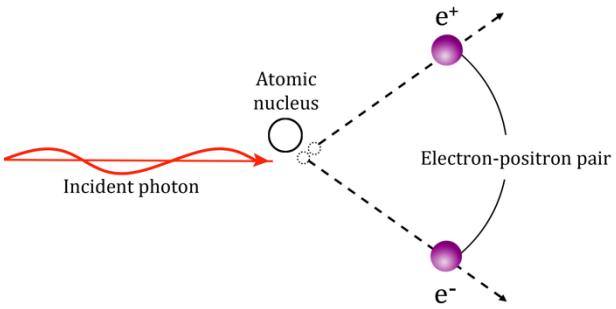

Fig. 3: Pair production process.

In a typical γ-ray spectrum, when the photon energy is higher than 1.02 MeV, a peak is always observed at 511 keV, usually called annihilation peak. In a NRF measurement, the intensity of this peak is large because many annihilation processes occur within the target material and then measured by the detector.

The pair production process has an impact on a NRF measurement in two aspects. First, the energy peaks in a NRF spectrum may be underestimated, especially when the resonating energy is high and the detector size is small. In this case, the incident photon with energy higher than 1.02 MeV, deposits an amount of energy inside the detector. The annihilation photons usually escape from the volume of the detector. Therefore, the energy deposited by the photon is decreased by an amount of 511 keV and 1.02 MeV when the single annihilation photon and the double annihilation photons escape from the detector respectively. As a result, the so-called the single escape and the double escape peaks appear in a NRF spectrum. These peaks can indicate the detection of the photo-peak especially when the main photo-peak is at high energy. Secondly, the appearance of the annihilation peak at 511 keV in all NRF spectra involving energy higher than 1.02 MeV provides an excellent means to produce a gating signal for the detectors.

1.1.4 Elastic scattering

The elastic (or coherent) scattering may be produced by more than one mechanism. In all of these mechanisms, when the incident photon hits an atom, the atom scatters the photons and returns to its initial state. The frequency of the scattered photon is exactly the same as the frequency of the incident photon. In terms of the available data, the cross sections of the elastic scattering are very small compared with that of the NRF. However, it represents a source of background that it is difficult, if not impossible, to be avoided. In contrast to the interactions mentioned above whose background effect is a count rate issue, the elastic scattering gives the same energy of the resonating photons at least

within the detector resolution. Therefore, the elastic scattering is the most severe source of background regarding NRF measurements.

As shown in Table 1, the elastic scattering includes the nuclear Thomson scattering, Rayleigh scattering and Delbrück scattering. Figure 4 shows illustration of the different mechanisms by which the elastic scattering takes place. Furthermore, at higher photon energies, *e.g.* > 5 MeV, a fourth mechanism is also present. This mechanism is called nuclear resonance scattering which comes from the low energy tail of the giant dipole resonance (GDR) [8].

An essential feature of the elastic scattering is that the differential cross section is proportional to the scattered amplitudes. Since there is a phase difference among the scattering amplitudes, all contributing processes may interfere in either a constructive or destructive manner. Consequently, accurate values of all scattering amplitudes due to all elastic scattering processes must be available in order to estimate the event rate of such interaction. Nevertheless, the commonly used elastic scattering cross section data only accounts for Rayleigh scattering.

Ignorance of the other elastics scattering processes such as Delbrück scattering may introduce a huge disagreement between the experimental measurements and theoretical predictions. For example, at E = 2.754 MeV, Z = 92 and θ = 90° the error due to restricting the elastic scattering on Rayleigh process is approximately 95%. This error is reduced to 49% by adding nuclear Thomson scattering and reduced to 6% by adding Delbrück scattering. Calculations of the differential cross section of the elastic scattering taking all processes into account is described in Section 2.

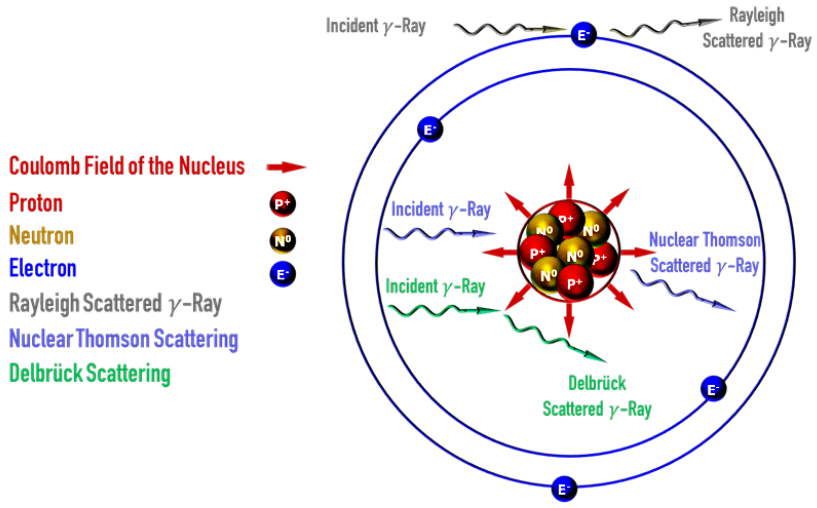

Fig. 4: Illustration of the elastic scattering mechanisms.

1.2 Cross sections

As an example of the wide range of the probability of occurrence of different γ-ray interactions, Fig. 5 shows the integrated cross section of all interactions described previously. The cross section is based on taken from the evaluated photon data library (EPDL) [9]. It is clear that up to ~ 200 keV, the total cross section is mainly from photoelectric absorption. Beyond this energy range, Compton (incoherent) scattering starts to be predominant up to 5 MeV. Furthermore, pair production process initiates at the threshold energy of 1.02 MeV and gets higher at higher energies.

The elastic (coherent) scattering has a small cross section in comparison to incoherent scattering around 2 ~ 3 MeV. However, data only represents the integrated cross section and therefore, no indication about the differential cross section can be inferred here. In Section 2, we shall show the differential cross section based on EPDL deviates far from the experimental observations.

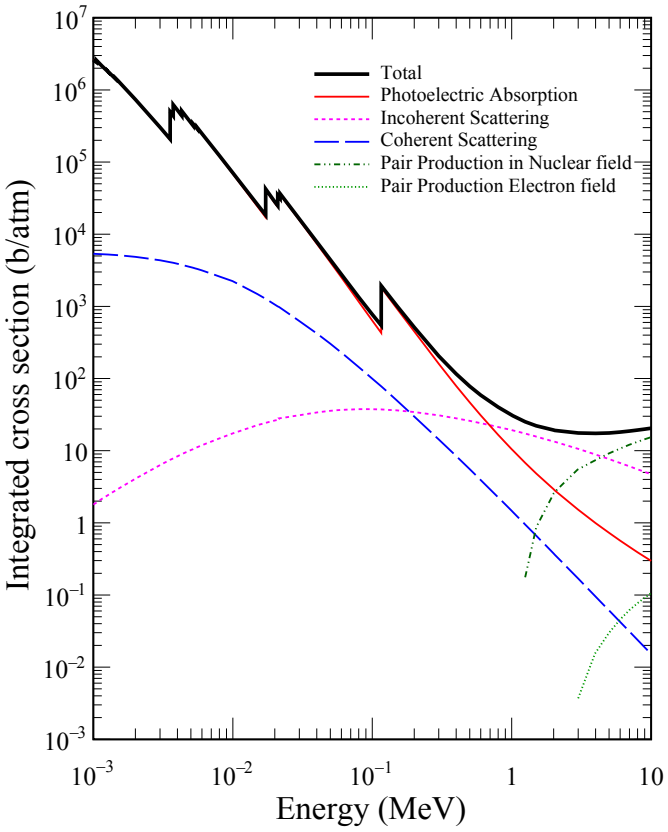

Fig. 5: Integrated cross section (over all angles) of the effective interactions up to 10 MeV in uranium [10].

1.3 EM interactions in Geant4

Table 2 shows the current status of the electromagnetic (EM) processes simulated in Geant4 [1, 11]. All the important interactions are simulated with many electromagnetic models. Each model has its own cross section data sets and sampling algorithm. The user may select the particular model that meets his requirements in terms of the validity of each model over a specific energy range. Nonetheless, many of these EM models provide excellent representations of the actual interactions.

The elastic scattering is simulated in Geant4 by considering Rayleigh scattering as the unique contributor to the total elastic scattering. Two main models are implemented in Geant4 for Rayleigh scattering as shown in Table 2, Livermore and Penelope models. Both models, however; exploit EPDL data which does not include all elastic scattering processes. Moreover, Rayleigh scattering cross section data is based on the form factor approximation. L. Kissel *et al.* provided a more accurate data based on the second order scattering matrix (S-matrix) [12]. Therefore, we developed a new simulation code for the elastic scattering using S-matrix data for Rayleigh scattering, first order born approximation for Delbrück scattering, and analytical functions for nuclear Thomson scattering as shown in the following sections.

Table 2: Electromagnetic Processes in Geant4 (10.3).

EM Process	EM Model
G4PhotoElectricEffect	G4PEEffectFluoModel; G4LivermorePhotoElectricModel G4LivermorePolarizedPhotoElectricModel; G4PenelopePhotoElectricModel
G4PolarizedPhotoElectricEffect	G4PolarizedPEEffectModel
G4ComptonScattering	G4KleinNishinaCompton; G4KleinNishinaModel; G4LivermoreComptonModel; G4LivermoreComptonModelRC G4LivermorePolarizedComptonModel; G4LowEPComptonModel; G4PenelopeComptonModel
G4PolarizedCompton	G4PolarizedComptonModel
G4GammaConversion	G4BetheHeitlerModel; G4PairProductionRelModel G4LivermoreGammaConversionModel; G4BoldyshevTripletModel; G4LivermoreNuclearGammaConversionModel; G4LivermorePolarizedGammaConversionModel; G4PenelopeGammaConvertionModel
G4PolarizedGammaConversion	G4PolarizedGammaConversionModel
G4RayleighScattering	G4LivermoreRayleighModel; G4LivermorePolarizedRayleighModel; G4PenelopeRayleighModel

2. Data preparation

The elastic scattering of γ-rays is not frequently dealt with among the various interactions of γ-ray with the matter because its probability of occurrence is small compared to other interactions, such as Compton scattering, in the MeV range. However; it has a significant role in a bunch of applications. Some examples of these applications are nuclear structure, homeland security and material characterization [13-16]. Literally, elastic scattering of γ-ray is an unavoidable background encountered in the photo-excitation of atomic nuclei, NRF. We have shown that the precise determination of the elastic scattering is an essential factor in the NDA of nuclear materials using NRF.

A comprehensive study on the simulation of the elastic scattering using Monte Carlo codes was conducted to evaluate the best cross section data-sets that agree with the experimental observations [17]. Although the study screened a large collection of experimental data points, it was limited to low energies, e.g., below 1 MeV. At such energy, the effect of Delbrück scattering could be ignored relative to Rayleigh scattering. Nevertheless; the study suggested that the S-matrix calculations for Rayleigh scattering amplitudes are more compatible with experimental data than the commonly used data based on the form factor approximation [17].

The current Data-Code Report provides a detailed description of the elastic scattering simulation code and illustrates the requirements needed to run this simulation including the data files. Other physics aspects and arguments behind the simulation are published elsewhere [2]. In the next section, we explain the methodology used in cross section data preparation. In section 3, the Geant4 implementation is described. In addition, an evaluation of the simulation code is presented. Supplementary materials, including cross section data and source code, will be attached to the current report. A brief description of these materials can be found in Appendix.

2.1 Differential cross section

Except the suggestion of Batiĉ *et al.* [17] to exploit the S-matrix calculations for Rayleigh scattering, all Monte Carol codes rely on the Evaluated Photon Data Library (EPDL) which is based on the form factor approximation. A comparison of EPDL data and experimental observations implies an imprecision, especially at high energy and large angle scattering, due to ignorance of other processes such as nuclear Thomson and Delbrück processes [2,17].

The differential cross section of the elastic scattering can be described in terms of the scattering amplitude A as,

$$\frac{d\sigma}{d\Omega} = |A|^2 \tag{7}$$

The resultant amplitude is the superposition of all elastic scattering amplitudes including Rayleigh (R), nuclear Thomson (T), Delbrück (D), and nuclear resonance (N). So that,

$$A = A^R + A^T + A^D + A^N \tag{8}$$

Each amplitude is expressed in terms of two components, with one in the direction of scattering plane, $A_{\parallel}$, and the other is perpendicular to it, $A_{\perp}$ [18]. Note that the scattering plane is defined by the momentum and the polarization vector of the incident photon. Details of the scattering geometry can be found in Ref. [18].

The differential cross section of un-polarized photon scattering is obtained by averaging over all polarizations of the incident and scattered photons,

$$\frac{d\sigma}{d\Omega} = \frac{1}{2}\left(\left|A_{\parallel}\right|^2 + |A_{\perp}|^2\right) \tag{9}$$

Sec. 2.2 shows how Rayleigh, A^R, and Delbrück, A^D, amplitudes are calculated from the available theoretical data. On the other hand, we ignore the nuclear resonance scattering process because its contribution is very small in the energy of interest. The final process is then nuclear Thomson scattering with its amplitude given by the classical Thomson scattering formula,

$$A_{\parallel}^T = -\frac{r_o Z^2 m}{M}, A_{\perp}^T = -\frac{r_o Z^2 m}{M} cos\theta \tag{10}$$

where m, M are the masses of electron and nucleus, respectively. r_o is the classical electron radius and θ is the scattering angle. The differential cross section is obtained by combining equations (7), (8), and (9) with the amplitudes given in the Sec. 2.2.

2.2 Interpolation of scattering amplitudes

Two sets of data are used to structure the data needed to run the simulation. The first set is called Rayleigh scattering database (RTAB) [19], while the second set gives Delbrück scattering amplitudes [20]. Both sets are given in tabular form according to the variation of the amplitudes with photon energy, scattering angle, and the atomic number of the scattering material. However; their data structures are not identical. Therefore, a unified data structure is required to establish a convenient data set for the simulation.

S.C. Roy *et al.* justified the interpolation process on the differential cross section of Rayleigh scattering using the S-matrix calculations as a primary source of data [21]. Here, we performed the interpolation process on the basic constitutes of the differential cross section, *i.e.* scattering amplitude. In such a case, more accurate data could be obtained. Our simulation code relies on a three-dimensional data grid in which the

differential cross section of the elastic scattering could be realized for the whole angular range and an energy range up to 3 MeV. The angular bin is 1° and the energy bin is 10 keV. Interpolation procedures have been applied on Rayleigh and Delbrück amplitudes.

RTAB data set consists of data files for all elements having $1 \leq Z \leq 99$. Each data file contains Rayleigh scattering amplitudes at different energies covering the whole angular range distributed non-uniformly over 97 angular points. Since Rayleigh scattering is peaked at forward directions, the distribution of the data is concentrated in the range $0° \leq \theta \leq 10°$. Regarding the energy of the incident photons, RTAB offers Rayleigh scattering amplitudes for 56 energy points starting from 54.3 eV to 2.754 MeV. 30% of these energy points are below 10 keV.

A dedicated class for the interpolation of Rayleigh and Delbrück amplitudes was implemented using the ROOT data analysis framework [22]. The interpolation was firstly performed on the scattering angle with 721 angles representing the whole angular range, *i.e.* $0° \leq \theta \leq 180°$ with a step of one-quarter of a degree. This relatively small angle step is essential at forward directions where the Rayleigh scattering amplitudes are changing rapidly. Thereafter, another interpolation process was made on the photon energy with an energy bin of 10 keV (300 energy points up to 3 MeV). Examples of Rayleigh amplitudes interpolation are shown in Fig. 6 – Fig.10 for different elements and photon energies.

The scattering amplitudes are expressed in terms of two right angle components as shown in Sec. 2.1. Moreover, each component of the scattering amplitudes is a complex number, which implies that Rayleigh scattering process is expressed by four scattering amplitudes. For example, as shown in Fig. 6 – Fig. 10, Rayleigh scattering amplitudes are $\mathrm{Re}\, a_{\parallel}^{\mathrm{R}}$ and $\mathrm{Im}\, a_{\parallel}^{\mathrm{R}}$ are the real and imaginary part of Rayleigh scattering amplitudes in a direction parallel to the incident photon polarization vector and $\mathrm{Re}\, a_{\perp}^{\mathrm{R}}$, and $\mathrm{Im}\, a_{\perp}^{\mathrm{R}}$ the real and imaginary part of Rayleigh scattering amplitudes in a direction perpendicular to the incident photon polarization vector.

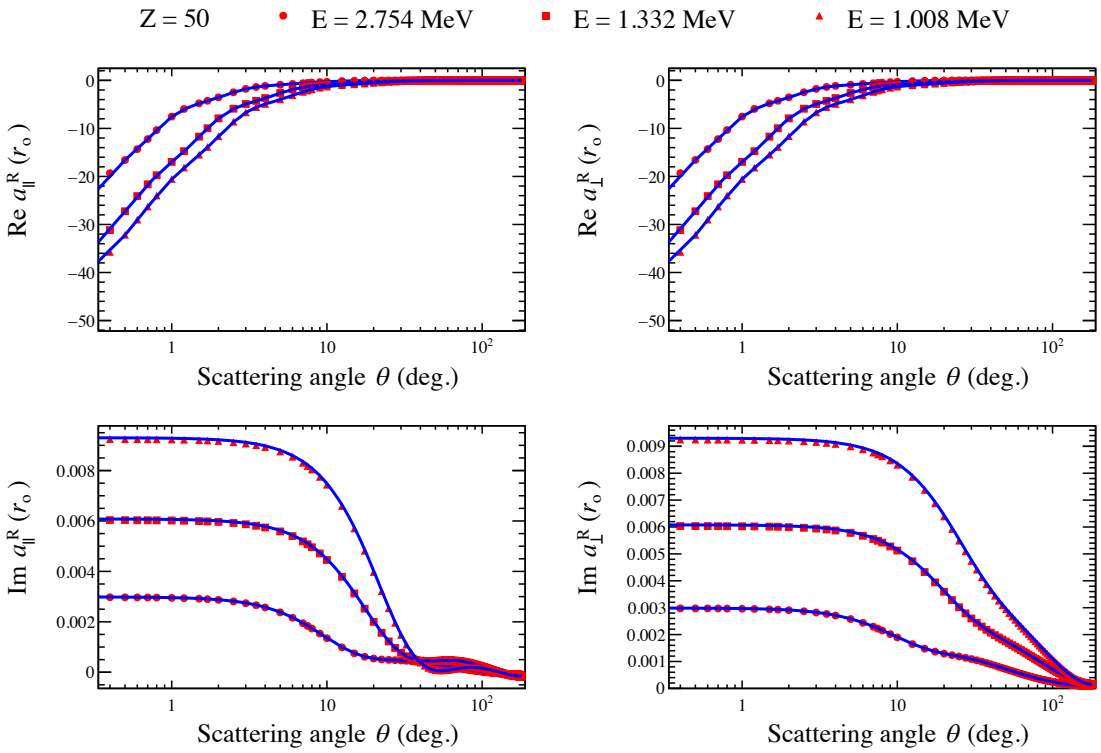

Fig. 6: Rayleigh scattering amplitudes taken from RTAB (points) with the interpolation function (lines) at different energies for tin ($Z = 50$).

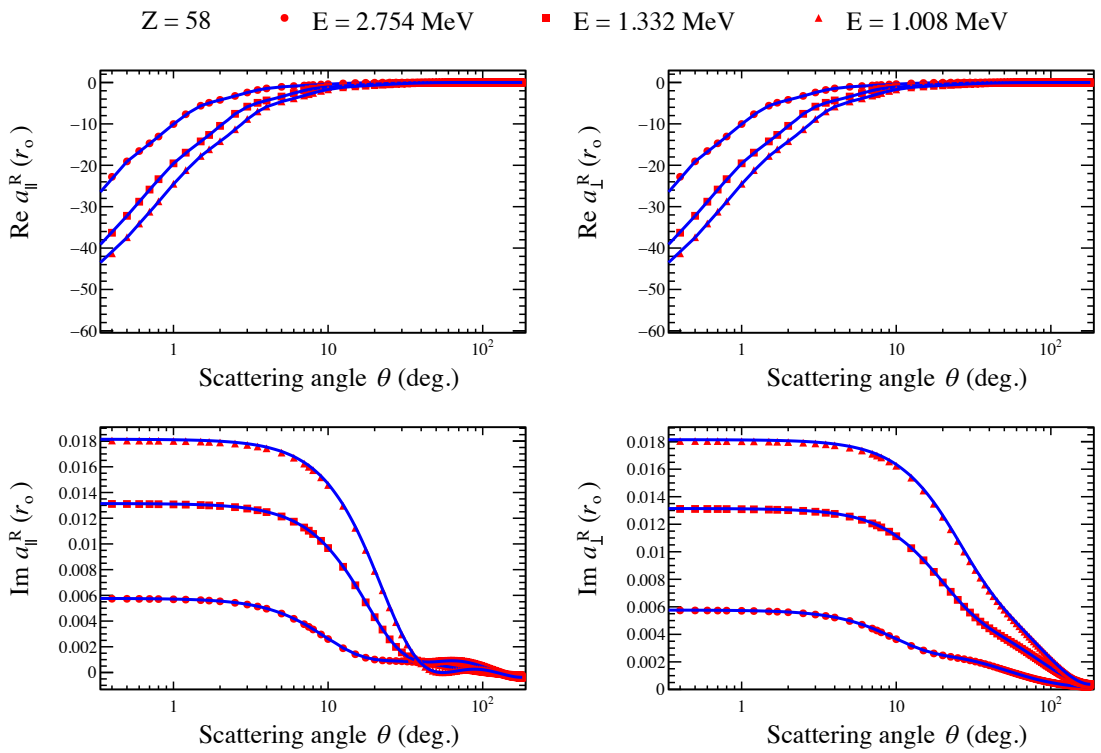

Fig. 7: Rayleigh scattering amplitudes taken from RTAB (points) with the interpolation function (lines) at different energies for cerium ($Z = 58$).

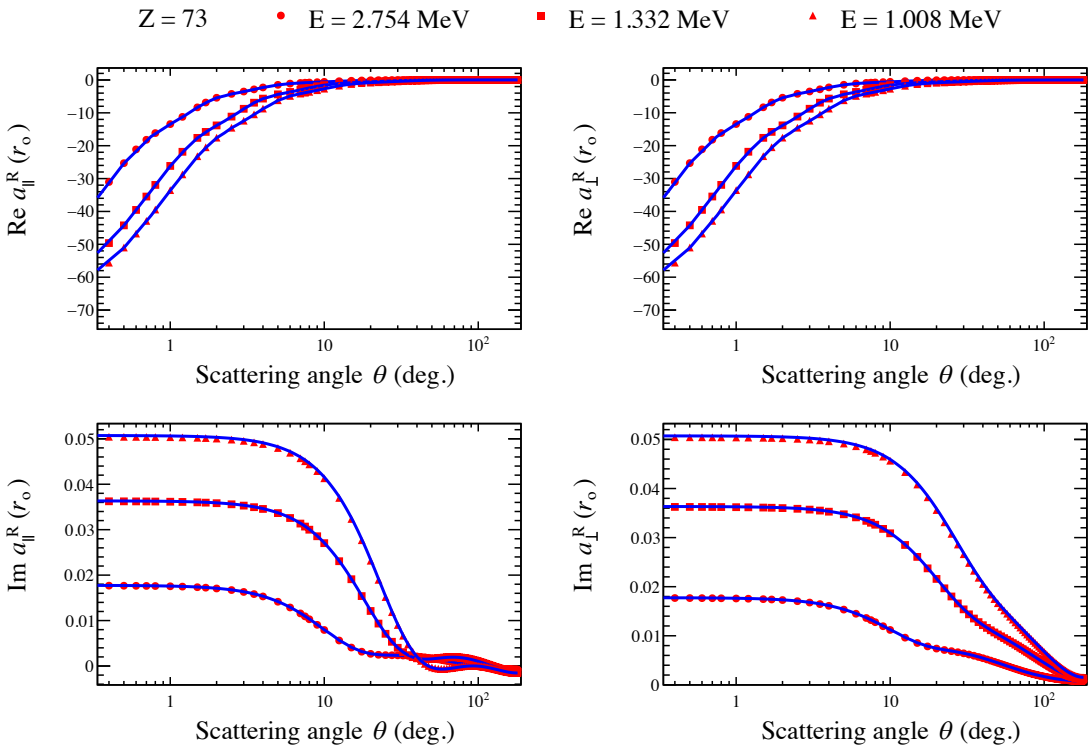

Fig. 8: Rayleigh scattering amplitudes taken from RTAB (points) with the interpolation function (lines) at different energies for tantalum ($Z = 73$).

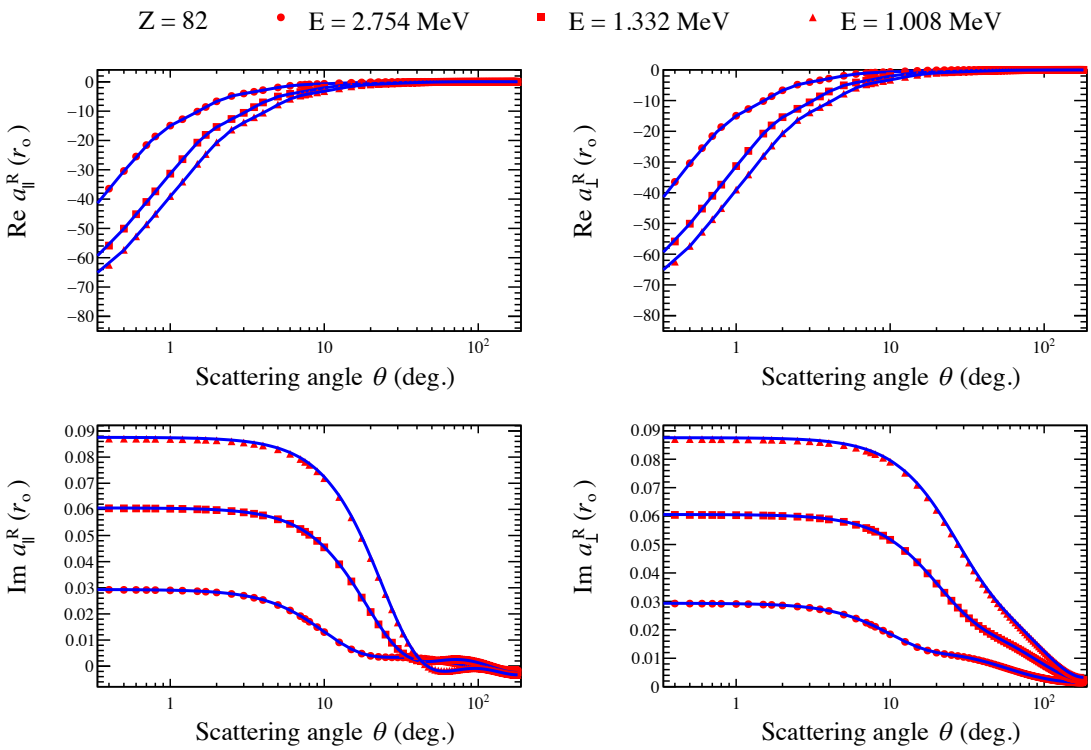

Fig. 9: Rayleigh scattering amplitudes taken from RTAB (points) with the interpolation function (lines) at different energies for lead ($Z = 82$).

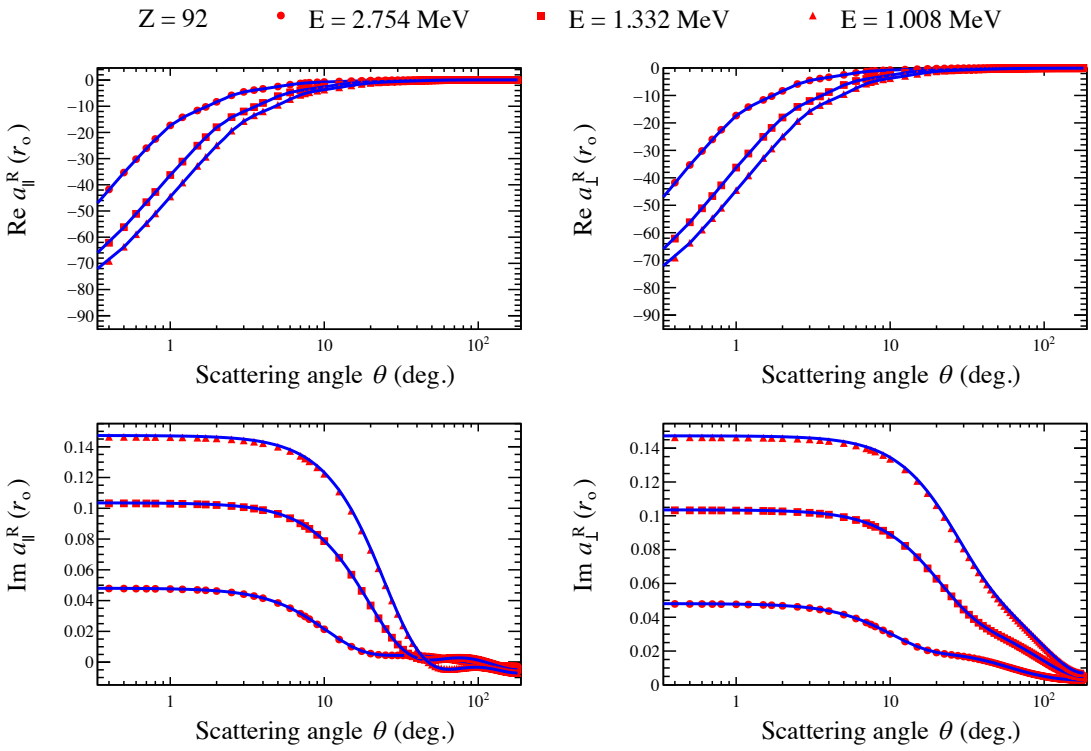

Fig. 10: Rayleigh scattering amplitudes taken from RTAB (points) with the interpolation function (lines) at different energies for uranium ($Z = 92$).

Unlike Rayleigh amplitudes, Delbrück amplitudes given by Falkenberg *et al.* [20] are tabulated for incident photon energy in the range 0.225 MeV ≤ E ≤ 2.754 MeV with 13 energy points. The angular range starts from 1° to 175° with some cases starting from 15° and other cases ending at 150°.

Moreover, Delbrück amplitudes at 0° are not available in the data provided by Falkenberg *et al.* [20]. Although Delbrück amplitudes are not rapidly changing as much as Rayleigh amplitudes at forward angles, accurate determination of 0° scattering amplitude is necessary. We used the optical theorem to overcome the forward angle Delbrück scattering in which the scattering amplitude depends only on the energy of the incident photon [23]. Extrapolation is performed for Delbrück scattering amplitudes in case of backward scattering, 180°.

Like the case of Rayleigh amplitudes, real and imaginary Delbrück amplitudes (Re $a_{\parallel}^{D}$, Im $a_{\parallel}^{D}$, Re $a_{\perp}^{D}$, and Im $a_{\perp}^{D}$) are plotted in Fig. 11 – Fig. 15 for different elements and at different angles. As shown in these figures, Delbrück amplitudes change smoothly with the scattering angle yielding an accurate interpolation and extrapolation using the available data points.

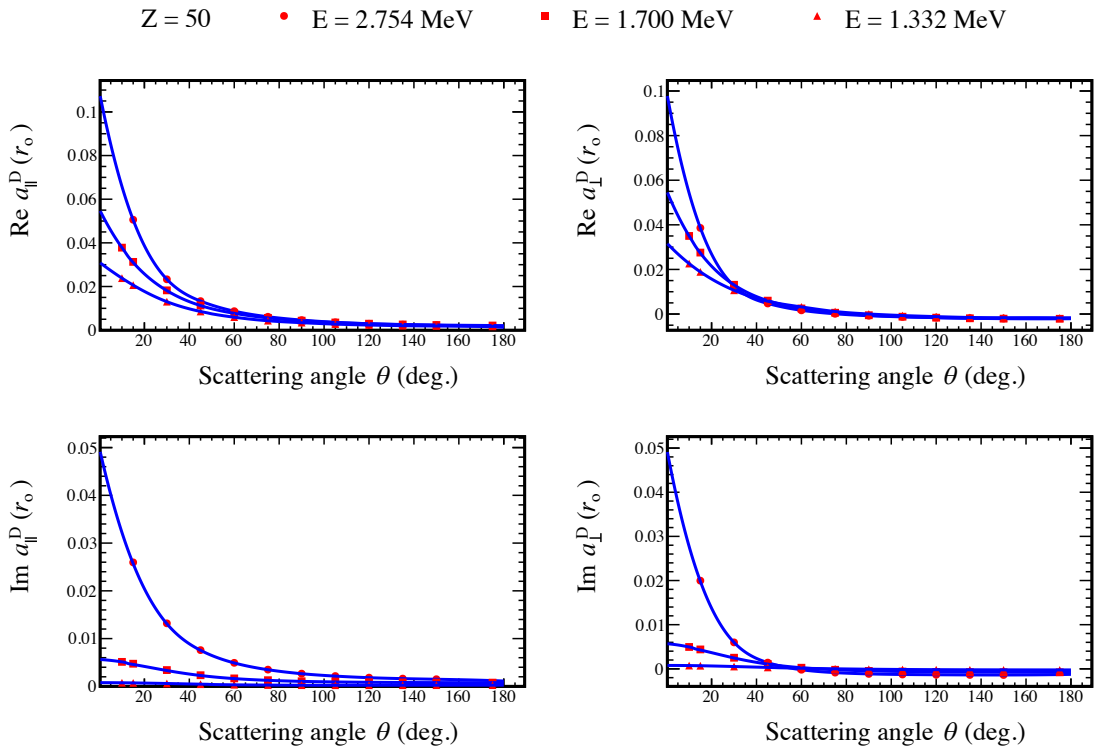

Fig. 11: Delbrück scattering amplitudes taken from Ref. [20] (points) with the interpolation function (lines) at different energies for tin ($Z = 50$).

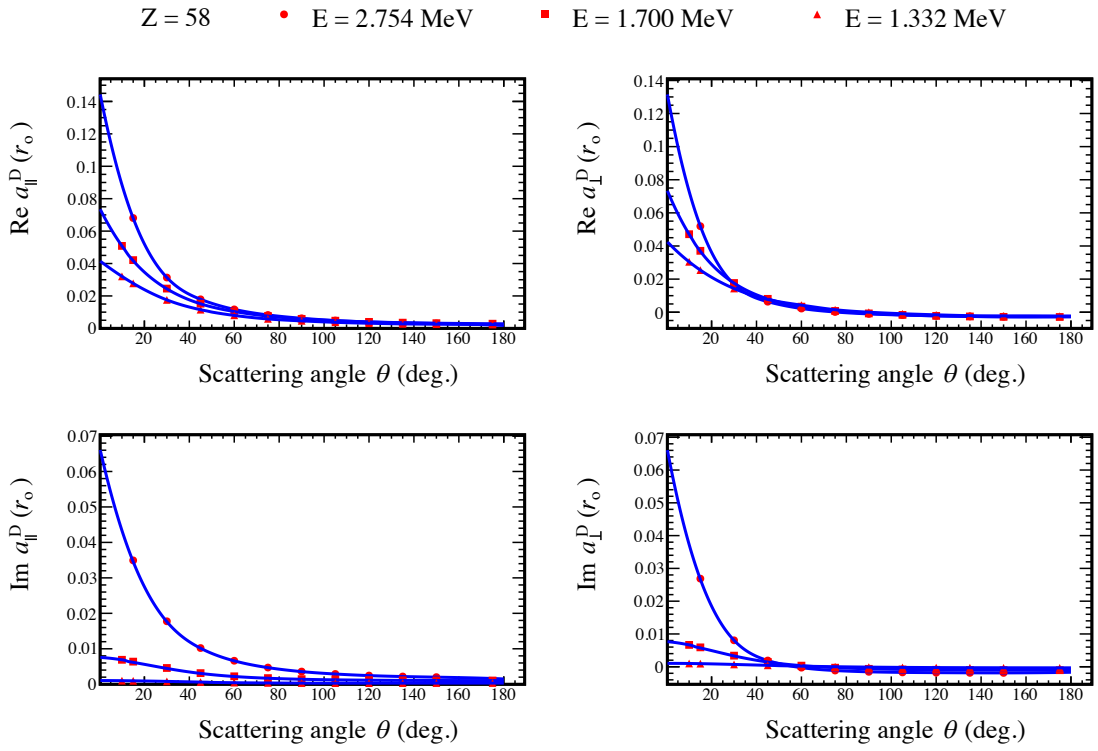

Fig. 12: Delbrück scattering amplitudes taken from Ref. [20] (points) with the interpolation function (lines) at different energies for cerium ($Z = 58$).

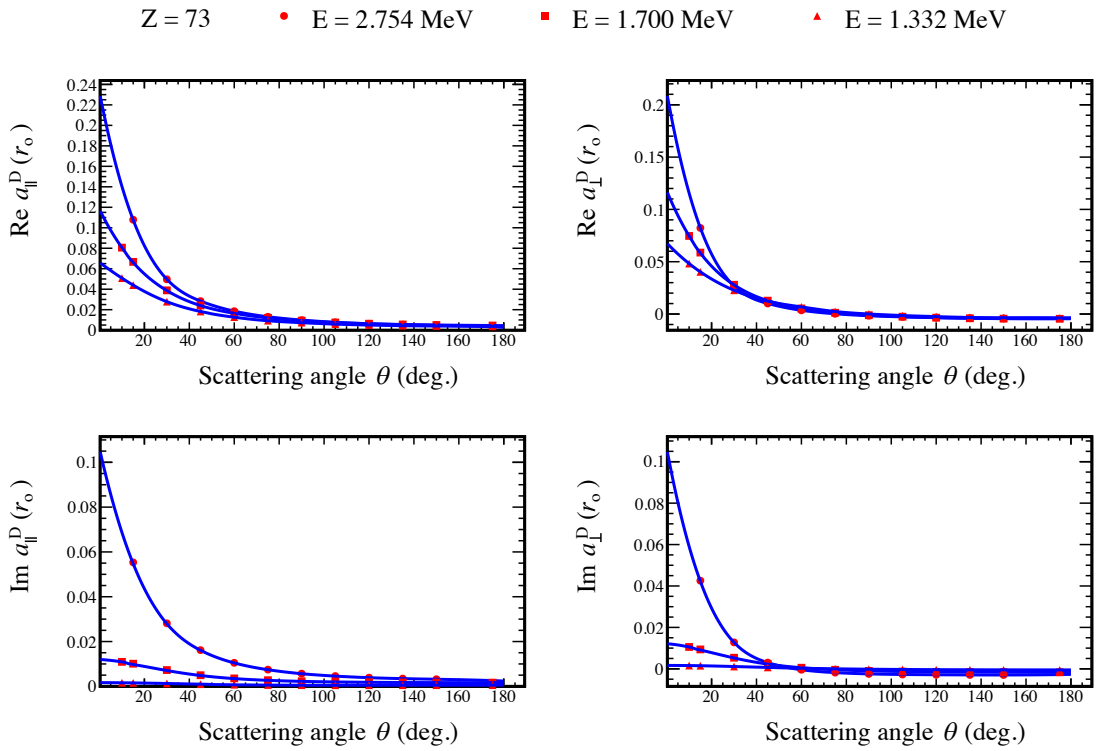

Fig. 13: Delbrück scattering amplitudes taken from Ref. [20] (points) with the interpolation function (lines) at different energies for tantalum ($Z = 73$).

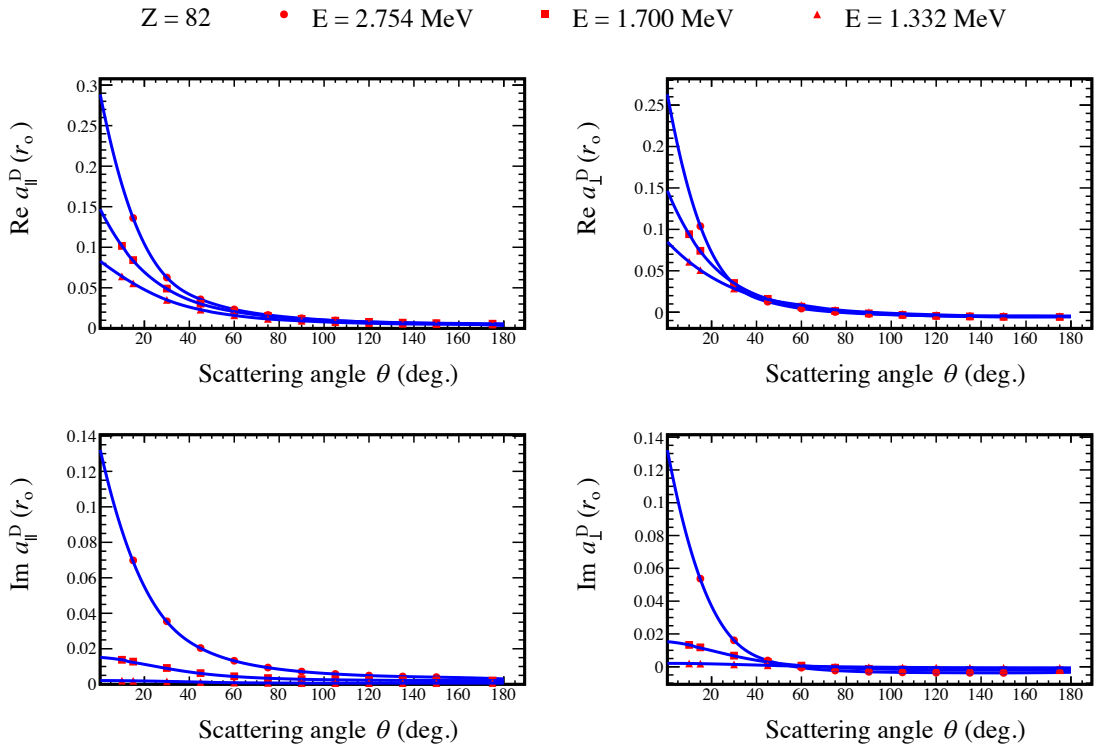

Fig. 14: Delbrück scattering amplitudes taken from Ref. [20] (points) with the interpolation function (lines) at different energies for lead ($Z = 82$).

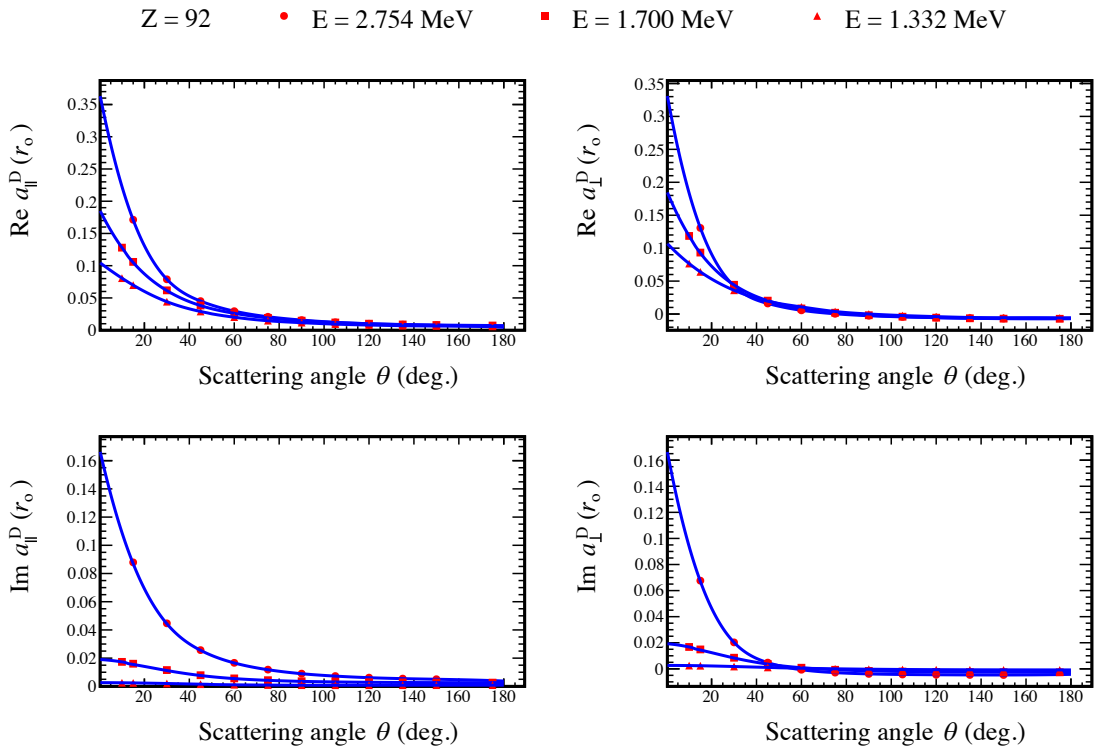

Fig. 15: Delbrück scattering amplitudes taken from Ref. [20] (points) with the interpolation function (lines) at different energies for uranium (Z = 92).

2.3 Integrated cross section

Generally, the differential cross section of elastic scattering is exploited as a probability distribution function in sampling the secondary species of an interaction within the simulation. On the other hand, the integrated cross section is used in sampling the probability of the interaction with respect to all other allowed interactions. Therefore, calculation of the integrated cross section is crucial for running the simulations. Owing to different scattering processes from different atomic species, all scattering amplitudes must superimpose before squaring. Since the elastic scattering of γ-rays is always peaked at forward directions, the effect of superposition is rather low on the integrated cross section.

Rayleigh and Delbrück amplitudes obtained in the Sec. 2.2 are used, along with nuclear Thomson amplitudes, to calculate the differential cross section at each energy. This differential cross section is integrated over all angles in order to provide a metric to sample the elastic scattering process. Numerical integration was performed over the 721 angular points at 300 energy points. The integration process is also performed for all elements prior the simulation. In order to benchmark our interpolation and numerical

integration, we compared the total cross section of elastic scattering with those published by L. Kissel *et al.* [12] and also with the EPDL calculations. Table 3 shows the integrated cross section for the elastic scattering of photons by lead at energies starting from 22.1 keV to 2750 keV. Since the total cross section provided by Ref. [12] are for Rayleigh and nuclear Thomson processes, we exclude Delbrück amplitude from this integrated cross section only for comparison purposes. The deviation between our integrated cross section and the Kissel's cross section is in the order of 1% and increases to 3% at low energy. This is in sharp contrast with the EPDL data which deviates up to 20% at high energy from our data.

In addition, we performed the integration of the differential cross section including Delbrück amplitudes. As an example, Fig. 16 shows our calculations of the integrated cross section of uranium in comparison with those retrieved from the EPDL. The inset of Fig. 16 illustrates the difference between the two data sets. In this inset a ratio of the integrated cross section calculated in this work (denoted as $\sigma_{tot.S-matrix}$) to that retrieved from EPDL (detonated as $\sigma_{tot.EPDL}$). The ratio increases with energy as the Delbrück scattering amplitudes become more effective. Moreover, the deviation depends on the phase difference between scattering amplitudes from different processes. Consequently, the deviation from the EPDL data may be positive or negative.

Table 3: Total cross section of elastic scattering in lead (Z = 82). Rayleigh scattering and nuclear Thomson scattering are only included.

Energy (keV)	Total cross section (b)		
	Ref. [12]	EPDL	This Work
2750	0.114	0.139	0.114
1330	0.484	0.588	0.491
1170	0.624	0.756	0.634
1120	0.684	0.824	0.691
889	1.08	1.30	1.09
662	1.94	2.29	1.96
412	4.97	5.68	5.03
279	10.6	11.8	10.7
145	35.8	38.4	36.5
75	94.2	118	97.7
59.5	150	171	153
22.1	695	708	727

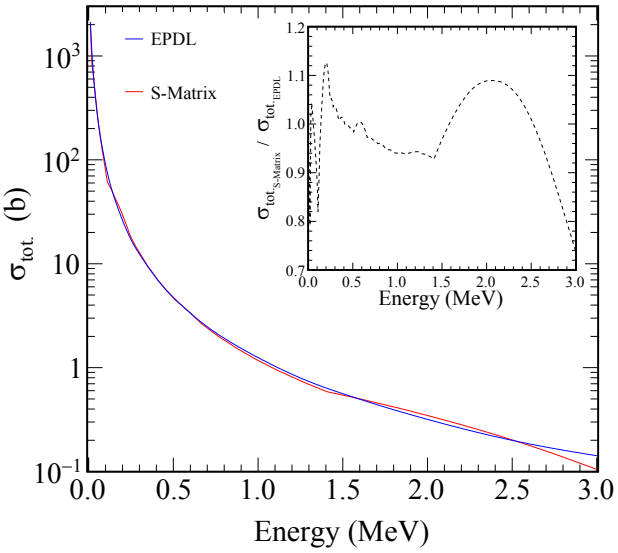

Fig. 16: Integrated cross section including Rayleigh, nuclear Thomson, and Delbrück scattering (blue) and the integrated cross section of coherent scattering retrieved from the EPDL (red).

It worth noting that the differential cross section has a greater effect on the simulation than the integrated cross section. This is because the elastic scattering is forward peaked and therefore, the integrated cross section is mainly a result of the forward angle scattering.

2.4 Data file structure

As mentioned earlier, differential and integrated cross sections are necessary parameters for running the simulation. Also, the way that these parameters are arranged and read throughout the simulation may affect the simulation accuracy and computational performance. Therefore, we deal with building data files very carefully. The primary grid size that the differential and integrated cross section are based on is 721 angular points time 300 energy points. Since this number is large, we reduce the grid size to 181 angular points and 300 energy points.

All required pieces of information are stored in a single data file per element. These files are invoked in the initialization phase of the simulation according to all materials involved in the simulation geometry. Both cross sections, integrated and differential, are tabulated at each energy and for all angles, respectively. A sample of data files is shown in Table 4. The table is constructed such that it contains 300 (representing the energy from 10 keV to 3 MeV) columns and 183 rows. The first row is the energy while the

second row is the integrated cross section at the corresponding energy. Rows from the third to 183rd represent the differential cross sections at the energy of the top for angles from 0° to 180°. Note that only a reduced version of such data file is depicted in Table 4.

Each data file contains approximately 54900 numbers, each of which is formatted in 13 characters. As a result, the uncompressed file size is about 714 KB. For all elements, the total uncompressed size of the whole database is about 70 MB. This size is comparable to the databases sizes encountered in a typical Geant4 physics model. However; the size of the database could be reduced to 29 MB by normal compression or by reducing the number of characters which numbers are formatted.

3. Coding

3.1 EM physics process in Geant4

In Geant4 simulation toolkit, electromagnetic processes such as Compton scattering, photoelectric effect or even elastic scattering can be realized by means of a common framework called G4EmProcess [24]. Each process may have different approaches to implementation, data sets, and valid ranges of energy. Depending on the user's interest, one can select the appropriate model via the so-called G4VEmModel [24]. In fact, G4VEmModel usually handles all the required pieces of physics information such as calculation of cross sections, sampling the process within a simulation run, and sampling secondary particles. For example, G4RayleighScattering is an abstract class derived from G4EmProcess while G4LivermoreRayleighModle or G4PenelopeRayelighModle can be invoked to simulate Rayleigh scattering.

Table 4: An example of a data file structure. The numbers are for uranium.

Energy (keV)	10	20	30	40	…	3000
Integrated cross section (b)	1.96E+03	8.15E+02	6.09E+02	4.11E+02	…	1.05E-01
Scattering Angle (deg.)	Differential cross section (b/st.)					
1	6.20E+02	5.76E+02	6.51E+02	6.58E+02	…	6.49E+02
2	6.19E+02	5.74E+02	6.46E+02	6.50E+02	…	1.54E+01
3	6.17E+02	5.68E+02	6.33E+02	6.28E+02	…	3.40E+00
4	6.14E+02	5.59E+02	6.14E+02	5.98E+02	…	7.44E-01
…	…	…	…	…	…	…
180	1.20E+02	2.64E+01	1.68E+01	9.59E+00	…	4.88E-05

3.2 JAEAElasticScattering process

Our simulation of the elastic scattering is based on implementing a new G4EmProcess with a new G4VEmModel. All classes and functions required for the process and the model were implemented and coded. Four files, which contain all classes and functions, were created. In the following, we shall describe the important functions within these files reasoning the methods used to implement the code. The complete versions of these files will be made available as supplementary materials along with this report.

3.2.1 Enumerator of the process

A new electromagnetic process in Geant4 must have enumerator which defines the sub-type of the process. All processes have their enumerators registered in the header file: G4EmProcessSubType.hh. According to the latest release of Geant4, 24 electromagnetic processes exist. So, enumerator of JAEAElasticScattering process is declared, in the header file JAEAElasticScatteringProcess.hh, following the existing processes as:

```
enum G4EmProcessSubType
{fJAEAElasticScattering=25};
```

3.2.2 Reading the data

As shown in Sec. 2, our simulation uses a special data set with a particular structure. Therefore, an implementation for reading the data is necessary. Reading the data required for the simulation is realized in the function JAEAElasticScattering-Model::ReadData. A global three-dimensional array is declared in the JAEAElastic-ScatteringModel such that to make this array visible within all the class's functions. Two dimensions of the array store differential and integrated cross sections and the corresponding energies while the third dimension is reserved for the atomic number of the element being selected randomly from the simulation geometry. Moreover, the path of which the data are retrieved is linked to the environment variable responsible for the Geant4 low energy data, G4LEDATA. The implementation of reading data is shown in the following box,

```
const char* datadir = path;
// Invoking the G4LEDATA environment variable.
  if(!datadir)
  {
```

```
    datadir = getenv("G4LEDATA");
    if(!datadir)
    {
      G4Exception("JAEAElasticScatteringModel::ReadData()","em0006",
          FatalException,
          "Environment variable G4LEDATA not defined");
      return;
    }
  }
// Get the data file path.
std::ostringstream ostCS;
ostCS << datadir << "/JAEAESData/cs_Z_" << Z <<".dat";
// Create data input buffer.
std::ifstream datainput(ostCS.str().c_str());
// Store data for a specific element.
while (!datainput.eof())
{
    for (int i=0; i<183;i++)
    {
        for (int j=0; j<300; j++)
        {
        data >> temp;
        data[Z][i][j] = temp;
        }
    }
    if (!datainput) break;
}
```

An additional task of the JAEAElasticScatteringModel::ReadData function is to prepare a continuous source of the integrated cross section at an arbitrary energy rather than the discrete values provided in the data file. This procedure is accomplished using the G4LPhysicsFreeVector() which is a special tool dedicated to handling cross section data. The main advantage of this vector is that it is capable of providing the integrated cross section at any energy by implying a fast interpolation algorithm.

```
std::ofstream fout("temp.txt", std::ofstream::out);
fout<<10e-3<<""<<3<<""<<300<<G4endl;
fout<<300<<G4endl;
```

```
fout<<scientific;
// Energy and integrated cross sections are stored in the first and // second
rows, respectively.
for (int i=0;i<300;i++)
// Unit conversion according to the Geant4 units.
    fout<<data[Z][0][i]*1e-3<<" "<<data[Z][1][i]*1e-22<<G4endl;
fout.close();
std::ifstream finCS("temp.txt");
 dataCS[Z] = new G4LPhysicsFreeVector();
// Activation of spline interpolation.
   dataCS[Z] ->SetSpline(true);
   dataCS[Z]->Retrieve(finCS, true);
```

3.2.3 Compute cross section

Sampling of an electromagnetic process in Geant4 is drawn according to the integrated cross section. The integrated cross section for the JAEAElasticScattering process is prepared as shown in Sec. 3.2.3. Nevertheless; the integrated cross section is assigned to the standard G4PhysicsVector in order to interpolate the integrated cross section depending on the photon energy. It worth noting that because the data grid is with good resolution, the interpolation would not degrade the accuracy of the total cross section.

3.2.4 Sampling secondary particles

Secondary particles in the elastic scattering process are only photons with the same energy as the incident photons and scattered at a direction determined by a probability distribution function. The sampling of secondary particles is performed using a function called JAEAElasticScatteringModel::SampleSecondaries. The main task of this function is to export the direction of scattered photon throughout the simulation. Depending on the energy of incident photon, the angular distribution function that will be used to sample the direction of the scattered photon is selected.

Since the resolution of the data grid is only 10 keV, a special procedure is followed to round the incident photon energy to the closest distribution within 5 keV. This procedure employs the C++ function of `lower_bound()` as shown below to increase the accuracy of the simulation. It should be emphasized that the probability of occurrence of the elastic scattering process is a continuous function owing to the interpolation made by the G4LPhysicsFreeVector as shown earlier. Since the elastic scattering cross section is a

slowly varying function of energy, the accuracy of selecting a probability distribution within 5 keV is quite satisfactory.

Once the angular distribution is correctly assigned, an inverse transform method can be applied to sample the scattered photon direction. The inverse transform requires a normalization of the probability distribution function (PDF). Then, the normalized PDF is used to calculate the cumulative distribution function (CDF). Finally, the CDF is employed with a uniform random number generator to produce the scattering angle according to the intended angular distribution. Finally, when the scattering angle is determined, the azimuth is uniformly sampled.

```
//Select the energy-grid point closest to the photon energy in keV
G4double *whichdistribution =
lower_bound(data[Z][0],data[Z][0]+300,photonEnergy0);
int index = max(0,(int)(whichdistribution-data[Z][0]-1));
//rounding up to half the energy-grid separation (5 keV)
if (photonEnergy0>=0.5*(data[Z][0][index]+data[Z][0][index+1]))
index++;
G4double normdist=0;
//normalization factor to create the probability distribution function
       for (int i=0;i<180;i++)
           {
           distribution[i]=data[Z][i+2][index];
           normdist = normdist + distribution[i];
           }
//Create the probability distribution function (pdf) and cumulative
distribution function (cdf)
       for (int i =0;i<180;i++) pdf[i]=distribution[i]/normdist;
       cdf[0]=0;
       G4double cdfsum =0;
       for (int i=0; i<180;i++)
           {
           cdfsum=cdfsum+pdf[i];
           cdf[i]=cdfsum;
           }
// Apply inverse transform
G4double r = G4UniformRand();
G4double *cdfptr=lower_bound(cdf,cdf+181,r);
```

```
int cdfindex = (int)(cdfptr-cdf-1);
G4double cdfinv = (r-cdf[cdfindex])/(cdf[cdfindex+1]-cdf[cdfindex]);
G4double theta = (cdfindex+cdfinv)/180.;
theta =theta*CLHEP::pi;
// Uniform azimuth
G4double phi = G4UniformRand()*2*CLHEP::pi;
```

3.3 Code evaluation methods

Two criteria were employed to evaluate the simulation code. The first criterion is to test the process against the reproduction of the differential cross section data (verification) and reproduction of the measured experimental results (validation). The second criterion is to assess the computational performance of the process in terms of the performance of similar processes in Geant4.

3.3.1 Verification and validation

To verify the JAEAElasticScatteringProcess, we simulated the angular distribution of the process using a dedicated example, namely TestEM14, attached in the latest Geant4 release. In this example, the user can activate any physics process of interest and extract the angular distribution of the secondary particles (in our case the scattered photons) created by the physics process. Furthermore, the example provides an easy modification of the simulation geometry by changing the scattering material via a macro-file.

We tested 5 elements in the range $50 \leq Z \leq 92$ using one billion events as primary (incident) photons with an energy of 2.754 MeV. The simulation results were then normalized and plotted with differential cross sections of the corresponding elements at the same energy of the incident photons. The histograms shown in Fig. 17 are the angular distributions of elastically scattered photons for different elements. The corresponding differential cross sections are overlaid as smooth curves. When comparing the simulation results with the differential cross section, we can see an excellent χ^2 as illustrated in Fig. 17. The very small values of χ^2 indicate that the JAEAElasticScatteringProcess can reproduce the input data efficiently. Despite the 4 keV difference between the incident photon energy (2.754 MeV) and the closest energy bin in the data grid (2.74 MeV), the angular distribution is correctly reproduced.

To validate the simulation by testing its ability to reproduce the experimental results, we designed a specific simulation by which a beam of photons is allowed to scatter elastically off a scatter and the scattered photons are recorded by a γ-ray detector. Since the photo-peak count in the detector is proportional to the differential cross section,

it may be possible to test the simulation code using experimental results from the literature. However; precise experimental conditions are usually not known. To overcome this problem, we proposed a ratio approach [2] so that we can compare a quote of the differential cross section relative to a reference element. In such a case, all parameters concerning the experimental conditions such as detector efficiency, thick target corrections, and detection geometry will be canceled out.

B. Kasten *et al.* measured the differential cross section of elastic scattering for the elements shown in Fig. 17 using the same apparatus [25]. If we define R_{exp} and R_{sim} as:

$$R_{exp} = \frac{Differential\ cross\ section\ of\ a\ reference\ element}{Differential\ cross\ section\ of\ the\ element\ of\ interest} \tag{11}$$

$$R_{sim} = \frac{Counts\ in\ photo-peak\ for\ a\ reference\ element}{Counts\ in\ photo-peak\ for\ the\ element\ of\ interest} \tag{12}$$

then, how equal the two ratios would be a metric for the validation of the simulation code. Table 5 shows the experimental differential cross section from Ref. [25], differential cross section used in our simulation, and the values of the two ratios R_{exp} and R_{sim}. It is clear that $R_{exp} \approx R_{sim}$ when the differential cross sections are very close. Equality of the two ratios indicates that the simulation code could reproduce the experimental results. It should be noted that there is approximately 6% difference between the experimental and theoretical differential cross sections at high Z elements.

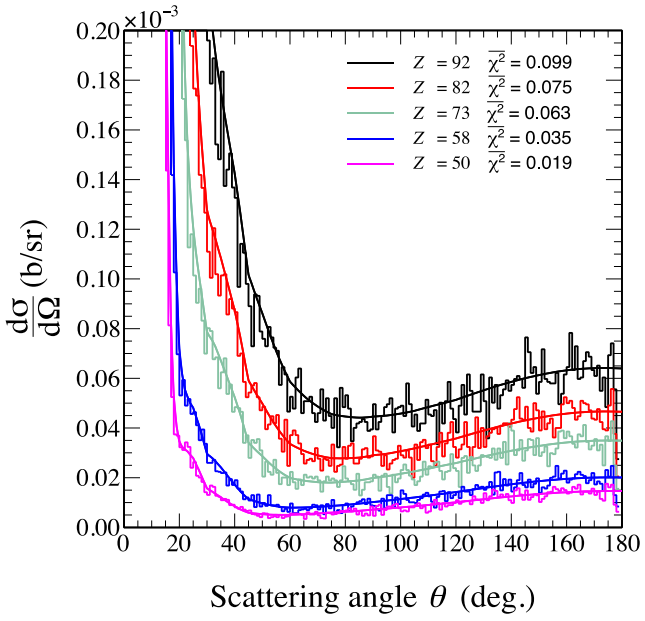

Fig. 17: Comparison between the angular distributions of elastically scattered 2.754 MeV photons, extracted from the simulation (histograms), and the differential cross section for different elements (smooth curves).

Table 5: Validation of the simulation code.

Z	$\frac{d\sigma}{d\Omega}^{exp}\left(\frac{\mu b}{sr.}\right)$	$\frac{d\sigma}{d\Omega}^{Data}\left(\frac{\mu b}{sr.}\right)$	R_{exp}	R_{sim}	$\frac{\lvert R_{exp}-R_{sim}\rvert}{R_{exp}}(\%)$
92	47.6 ± 3.1	44.7	0.14 ± 0.012	0.17	21
82	31.0 ± 1.6	29.0	0.21 ± 0.016	0.26	24
73	19.2 ± 0.60	19.9	0.34 ± 0.019	0.33	3.0
58	10.6 ± 0.33	10.2	0.63 ± 0.034	0.68	8.0
50	6.62 ± 0.15	7.10	1.00 ± 0.045	1.00	0.0

Although the difference is less than the experimental uncertainty, its systematic appearance only at high Z may be attributed to the Coulomb correction to Delbrück amplitudes. These corrections are made in higher orders of Born approximation and they are not taken into account in our data for Delbrück amplitudes [2].

3.3.2 Computational performance

The execution time of a simulation is a crucial indicator about the goodness of the code. Even with the high-performance computational capabilities, the simulation should be executed within a practical timeframe. To assess our simulation model, we compare its computational performance with those of similar Geant4 models, e.g., G4LivermoreRayleighModel and G4PenelopeRayleighModel.

A microsecond timer is started at the main function of an example that uses JAEAElasticScatteringModel, G4LivermoreRayleighModel, or G4PenelopeRaylighModel. This timer is declared using the C++ function `gettimeofday()`. Timestamps at different parts of the code are established by invoking the timer at arbitrary points within the code. These points start from the initialization of the process to the end of the simulation. A total number of 8 timestamps provide a reasonable determination of the computational performance.

```
// Declaring the timer
// Each time the timer is invoked, both time.tv_sec and time.tv_usec are
stored to determine the exact second when timer is invoked.
gettimeofday(&start_time, NULL);
SW_s = start_time.tv_sec;
SW_us = start_time.tv_usec;
```

The initialization time is defined as the time required to read data and compute cross sections needed for the simulation. The initialization time is averaged over a total number of 20 simulation runs. The sampling time is the time difference between the start and the end of SmapleSecondaries function. For accurate determination of the sampling time, the time is averaged twice. First, the sampling time is averaged over 10 million events within a simulation run. The simulation is run for 20 times with the same number of primary events and then the sampling time is averaged again over the number of the simulations runs. This procedure is repeated for the three processes mentioned above. Table 6 shows the initialization and sampling times for the three processes along with the memory footprint of each process.

All simulation runs devoted for measuring the computational performance were executed on a single core of a 4 GHz Intel Core i7-4790K processor with a Geant4 10.3.1 installed on a Scientific Linux virtual machine. It is clear from Table 6 that the computational performance of JAEAElasticScatteringModel is compatible with the similar implementations in Geant4. There is almost no difference in the initialization time. However; JAEAElasticScatteringModel is slower than the current models in Geant4 in terms of sampling time. On the other hand, JAEAElasticScatteringModel provides the most accurate representation of the elastic scattering of γ-rays.

Table 6: Computational performance of our process in comparison to similar Geant4 processes.

Process	Initialization time (s)	Sampling time per event (μ s)	Memory footprint (MB)
JAEAElasticScatteringModel	0.42 ± 0.03	2.57 ± 0.06	24.3 ± 1.54
G4PenelopeRayleighModel	0.43 ± 0.05	1.99 ± 0.08	21.4 ± 1.04
G4LivermoreRayleighModel	0.41 ± 0.02	2.14 ± 0.09	21.3 ± 0.93

4. Summary

We developed a new Geant4 physics process to simulate the elastic scattering of γ-rays up to 3 MeV. Owing to the inclusion of scattering amplitudes due to all effective scattering phenomena; namely Rayleigh, nuclear Thomson, and Delbrück amplitudes, the simulation provides an accurate representation of the total elastic scattering of γ-rays. Code implementations and data required to run the simulation were described. Tests over 5 elements showed that the simulation is verified and validated over the anticipated energy range. Furthermore, the simulation results indicated that the newly developed process consumes a reasonable execution time which is comparable to

execution times encountered in Geant4. The process and the model were derived from G4EmProcess and G4VEmModel, respectively. Therefore, the process can be run under Geant4.10.3 and next releases. The simulation code can be easily extended to higher energies once the corresponding data is made available.

Appendix

Supplementary materials are attached with the present report. These materials include the following items:

1. Source code which includes the following files:
   - Source code
     - JAEAElasticScattering.cc
     - JAEAElasticScattering.hh
     - JAEAElasticScatteringModel.cc
     - JAEAElasticScatteringModel.hh
2. Data files: Data files required to run the simulation are 99 files for all elements having $1 \leq Z \leq 99$. A readme file is also attached to describe the structure of the data file.
   - JAEAESData
     - cs_Z_1.dat
     - cs_Z_2.dat
     - cs_Z_3.dat
     - …
     - cs_Z_99.dat
   - README

Acknowledgements

This work was supported by Ministry of Education, Culture, Sports, Science and Technology (MEXT), Japan.

References

[1] S. Agostinelli et al., GEANT4- a simulation toolkit, Nucl. Instrum. Methods Phys. Res. Sect. A, vol. 506, 2003, pp. 250-303.

[2] M. Omer, R. Hajima, Including Delbrück scattering in Geant4, Nucl. Instrum. Methods Phys. Res. Sect. B, vol. 405, 2017, pp. 43-49.

[3] R.D. Evans, *The atomic nucleus*, THM Edition, McGraw-Hill, Inc., 1955, pp. 672-710.

[4] U. Fano, Gamma ray attenuation part 1: basic process, Nucleonics, vol. 11, no.8, 1953, pp. 8-12.

[5] U. Fano, Gamma ray attenuation part 2: analysis of penetration, Nucleonics, vol. 11, no. 9, 1953, pp. 55-61.

[6] R.D. Evans, in *American Institute of Physics Handbook*, 3rd ed. Ed. D.E. Gray, McGraw-Hill Inc., 1972, pp. 8/190-218.

[7] O. Klein, Y. Nishina, Über die Streuung von Strahlung durch freie Elektronen nach der neuen relativistischen Quantendynamik von Dirac, Z. Physik, vol. 52, 1929, pp. 853-868.

[8] M. Schumacher et al., The energy dependence of Delbrück scattering investigated at Z = 73, 82 and 92, Nucl. Phys. A, vol. 346, no. 3, 1980, pp. 418-430.

[9] D.E. Cullen, J.H. Hubbell, L. Kissel, EPDL97: The Evaluated Photon Data Library '97 Version, Lawrence Livermore National Laboratory Rep. UCRL-LR-50400, vol. 6, 1997, pp. 1-28.

[10] M.J. Berger et al., XCOM: Photon Cross Section Database, National Institute of Standards and Technology, http://physics.nist.gov/xcom (accessed 2017/09/29).

[11] Geant4 Collaboration, Physics Reference Manual, Geant4 10.3, 2016, pp.1-563.

[12] L. Kissel, R.H. Pratt, S.C. Roy, Rayleigh scattering by neutral atoms, 100 eV to 10 MeV, Phys. Rev. A, vol. 22, no. 5, 1980, pp. 1970-2004.

[13] R.H. Pratt, Photon absorption and photon scattering – what we do not know and why it matters, Radiat. Phys. Chem., vol. 95, 2014, pp. 4-13.

[14] J.H. Hubbell, Review and history of photon cross section calculations, Phys. Med. Biol., vol. 51, no. 13, 2006, pp. R245-R262.

[15] M. Omer et al., Nuclear Resonance Fluorescence of ^{235}U Measured with High-Resolution $LaBr_3$(Ce) Scintillation Detectors, Jpn. J. Appl. Phys., vol. 52, no. 10R, 2013, pp. 106401/1-4.

[16] M. Omer et al., Analysis of nuclear resonance fluorescence excitation measured with $LaBr_3$(Ce) detectors near 2 MeV, Nucl. Instrum. Methods Phys. Res. Sect. A, vol. 729, 2013, pp. 102-107.

[17] M. Batiĉ, G. Hoff, M.G. Pia, P. Saracco, Photon Elastic Scattering Simulation:

Validation and Improvements to Geant4, IEEE Trans. Nucl. Sci., vol. 59, no. 4, 2012, pp. 1636-1664.

[18] L. Kissel, R.H. Pratt, in: B. Crasemann (Ed.), *Atomic Inner-Shell Physics*, Plenum Press, 1985, pp. 465-532.

[19] L. Kissel, RTAB: the Rayleigh scattering database, Radiat. Phys. Chem., vol. 59, no. 2, 2000, pp. 185-200.

[20] H. Falkenberg, A. Hünger, P. Rullhusen, M. Schumacher, Amplitudes for Delbrück scattering, At. Data Nucl. Data Tables, vol. 50, no. 1, 1992, pp. 1-27.

[21] S.C. Roy, L. Kissel, R.H. Pratt, Elastic scattering of photons, Radiat. Phys. Chem., vol. 56, no.1-2, 1999, pp. 3-26.

[22] R. Brun, F. Rademakers, ROOT – An object oriented data analysis framework, Nucl. Instrum. Methods Phys. Res. Sect. A, vol. 389, no. 1-2, 1997, pp. 81-86.

[23] F. Rohrlich, R.L. Gluckstern, Forward Scattering of Light by a Coulomb Field, Phys. Rev., vol. 86, no. 1, 1952, pp. 1-9.

[24] Geant4 Collaboration, Geant4 User's Guide for Application Developers, Geant4 10.2, 2015, pp. 1-385.

[25] B. Kasten, et al., Coulomb correction effect in Delbrück scattering and atomic Rayleigh scattering of 1-4 MeV photons, Phys. Rev. C, vol. 33, no. 5, 1986, pp. 1606-1615.

国際単位系（SI）

表１．SI 基本単位

基本量	SI 基本単位	
	名称	記号
長さ	メートル	m
質量	キログラム	kg
時間	秒	s
電流	アンペア	A
熱力学温度	ケルビン	K
物質量	モル	mol
光度	カンデラ	cd

表２．基本単位を用いて表されるSI組立単位の例

組立量	SI 組立単位	
	名称	記号
面積	平方メートル	m^2
体積	立方メートル	m^3
速さ，速度	メートル毎秒	m/s
加速度	メートル毎秒毎秒	m/s^2
波数	毎メートル	m^{-1}
密度，質量密度	キログラム毎立方メートル	kg/m^3
面積密度	キログラム毎平方メートル	kg/m^2
比体積	立方メートル毎キログラム	m^3/kg
電流密度	アンペア毎平方メートル	A/m^2
磁界の強さ	アンペア毎メートル	A/m
量濃度(a)，濃度	モル毎立方メートル	mol/m^3
質量濃度	キログラム毎立方メートル	kg/m^3
輝度	カンデラ毎平方メートル	cd/m^2
屈折率(b)	（数字の） 1	1
比透磁率(b)	（数字の） 1	1

(a) 量濃度（amount concentration）は臨床化学の分野では物質濃度（substance concentration）ともよばれる。
(b) これらは無次元量あるいは次元１をもつ量であるが、そのことを表す単位記号である数字の１は通常は表記しない。

表３．固有の名称と記号で表されるSI組立単位

組立量	SI 組立単位			
	名称	記号	他のSI単位による表し方	SI基本単位による表し方
平面角	ラジアン(b)	rad	1 (b)	m/m
立体角	ステラジアン(b)	sr(c)	1 (b)	m^2/m^2
周波数	ヘルツ(d)	Hz		s^{-1}
力	ニュートン	N		m kg s^{-2}
圧力，応力	パスカル	Pa	N/m^2	m^{-1} kg s^{-2}
エネルギー，仕事，熱量	ジュール	J	N m	m^2 kg s^{-2}
仕事率，工率，放射束	ワット	W	J/s	m^2 kg s^{-3}
電荷，電気量	クーロン	C		s A
電位差（電圧），起電力	ボルト	V	W/A	m^2 kg s^{-3} A^{-1}
静電容量	ファラド	F	C/V	m^{-2} kg^{-1} s^4 A^2
電気抵抗	オーム	Ω	V/A	m^2 kg s^{-3} A^{-2}
コンダクタンス	ジーメンス	S	A/V	m^{-2} kg^{-1} s^3 A^2
磁束	ウエーバ	Wb	Vs	m^2 kg s^{-2} A^{-1}
磁束密度	テスラ	T	Wb/m^2	kg s^{-2} A^{-1}
インダクタンス	ヘンリー	H	Wb/A	m^2 kg s^{-2} A^{-2}
セルシウス温度	セルシウス度(e)	℃		K
光束	ルーメン	lm	cd sr(c)	cd
照度	ルクス	lx	lm/m^2	m^{-2} cd
放射性核種の放射能(f)	ベクレル(d)	Bq		s^{-1}
吸収線量，比エネルギー分与，カーマ	グレイ	Gy	J/kg	m^2 s^{-2}
線量当量，周辺線量当量，方向性線量当量，個人線量当量	シーベルト(g)	Sv	J/kg	m^2 s^{-2}
酸素活性	カタール	kat		s^{-1} mol

(a)SI接頭語は固有の名称と記号を持つ組立単位と組み合わせても使用できる。しかし接頭語を付した単位はもはやコヒーレントではない。
(b)ラジアンとステラジアンは数字の１に対する単位の特別な名称で、量についての情報をつたえるために使われる。実際には、使用する時には記号radおよびsrが用いられるが、習慣として組立単位としての記号である数字の１は明示されない。
(c)測光学ではステラジアンという名称と記号srを単位の表し方の中に、そのまま維持している。
(d)ヘルツは周期現象についてのみ、ベクレルは放射性核種の統計的過程についてのみ使用される。
(e)セルシウス度はケルビンの特別な名称で、セルシウス温度を表すために使用される。セルシウス度とケルビンの単位の大きさは同一である。したがって、温度差や温度間隔を表す数値はどちらの単位で表しても同じである。
(f)放射性核種の放射能（activity referred to a radionuclide）は、しばしば誤った用語で"radioactivity"と記される。
(g)単位シーベルト（PV,2002,70,205）についてはCIPM勧告2（CI-2002）を参照。

表４．単位の中に固有の名称と記号を含むSI組立単位の例

組立量	SI 組立単位		
	名称	記号	SI 基本単位による表し方
粘度	パスカル秒	Pa s	m^{-1} kg s^{-1}
力のモーメント	ニュートンメートル	N m	m^2 kg s^{-2}
表面張力	ニュートン毎メートル	N/m	kg s^{-2}
角速度	ラジアン毎秒	rad/s	m m^{-1} s^{-1}=s^{-1}
角加速度	ラジアン毎秒毎秒	rad/s^2	m m^{-1} s^{-2}=s^{-2}
熱流密度，放射照度	ワット毎平方メートル	W/m^2	kg s^{-3}
熱容量，エントロピー	ジュール毎ケルビン	J/K	m^2 kg s^{-2} K^{-1}
比熱容量，比エントロピー	ジュール毎キログラム毎ケルビン	J/(kg K)	m^2 s^{-2} K^{-1}
比エネルギー	ジュール毎キログラム	J/kg	m^2 s^{-2}
熱伝導率	ワット毎メートル毎ケルビン	W/(m K)	m kg s^{-3} K^{-1}
体積エネルギー	ジュール毎立方メートル	J/m^3	m^{-1} kg s^{-2}
電界の強さ	ボルト毎メートル	V/m	m kg s^{-3} A^{-1}
電荷密度	クーロン毎立方メートル	C/m^3	m^{-3} s A
表面電荷	クーロン毎平方メートル	C/m^2	m^{-2} s A
電束密度，電気変位	クーロン毎平方メートル	C/m^2	m^{-2} s A
誘電率	ファラド毎メートル	F/m	m^{-3} kg^{-1} s^4 A^2
透磁率	ヘンリー毎メートル	H/m	m kg s^{-2} A^{-2}
モルエネルギー	ジュール毎モル	J/mol	m^2 kg s^{-2} mol^{-1}
モルエントロピー，モル熱容量	ジュール毎モル毎ケルビン	J/(mol K)	m^2 kg s^{-2} K^{-1} mol^{-1}
照射線量（X線及びγ線）	クーロン毎キログラム	C/kg	kg^{-1} s A
吸収線量率	グレイ毎秒	Gy/s	m^2 s^{-3}
放射強度	ワット毎ステラジアン	W/sr	m^4 m^{-2} kg s^{-3}=m^2 kg s^{-3}
放射輝度	ワット毎平方メートル毎ステラジアン	$W/(m^2$ sr)	m^2 m^{-2} kg s^{-3}=kg s^{-3}
酵素活性濃度	カタール毎立方メートル	kat/m^3	m^{-3} s^{-1} mol

表５．SI 接頭語

乗数	名称	記号	乗数	名称	記号
10^{24}	ヨタ	Y	10^{-1}	デシ	d
10^{21}	ゼタ	Z	10^{-2}	センチ	c
10^{18}	エクサ	E	10^{-3}	ミリ	m
10^{15}	ペタ	P	10^{-6}	マイクロ	μ
10^{12}	テラ	T	10^{-9}	ナノ	n
10^{9}	ギガ	G	10^{-12}	ピコ	p
10^{6}	メガ	M	10^{-15}	フェムト	f
10^{3}	キロ	k	10^{-18}	アト	a
10^{2}	ヘクト	h	10^{-21}	ゼプト	z
10^{1}	デカ	da	10^{-24}	ヨクト	y

表６．SIに属さないが、SIと併用される単位

名称	記号	SI 単位による値
分	min	1 min=60 s
時	h	1 h =60 min=3600 s
日	d	1 d=24 h=86 400 s
度	°	1°=(π/180) rad
分	’	1’=(1/60)°=(π/10 800) rad
秒	”	1”=(1/60)’=(π/648 000) rad
ヘクタール	ha	1 ha=1 hm^2=10^4m^2
リットル	L, l	1 L=1 l=1 dm^3=10^3cm^3=$10^{-3}m^3$
トン	t	1 t=10^3 kg

表７．SIに属さないが、SIと併用される単位で、SI単位で表される数値が実験的に得られるもの

名称	記号	SI 単位で表される数値
電子ボルト	eV	1 eV=1.602 176 53(14)×10^{-19}J
ダルトン	Da	1 Da=1.660 538 86(28)×10^{-27}kg
統一原子質量単位	u	1 u=1 Da
天文単位	ua	1 ua=1.495 978 706 91(6)×10^{11}m

表８．SIに属さないが、SIと併用されるその他の単位

名称	記号	SI 単位で表される数値
バール	bar	1 bar=0.1MPa=100 kPa=10^5Pa
水銀柱ミリメートル	mmHg	1 mmHg≈133.322Pa
オングストローム	Å	1 Å=0.1nm=100pm=10^{-10}m
海里	M	1 M=1852m
バーン	b	1 b=100fm^2=(10^{-12}cm)^2=$10^{-28}m^2$
ノット	kn	1 kn=(1852/3600)m/s
ネーパ	Np	SI単位との数値的な関係は、対数量の定義に依存。
ベル	B	
デシベル	dB	

表９．固有の名称をもつCGS組立単位

名称	記号	SI 単位で表される数値
エルグ	erg	1 erg=10^{-7} J
ダイン	dyn	1 dyn=10^{-5}N
ポアズ	P	1 P=1 dyn s cm^{-2}=0.1Pa s
ストークス	St	1 St =1cm^2 s^{-1}=$10^{-4}m^2$ s^{-1}
スチルブ	sb	1 sb =1cd cm^{-2}=10^4cd m^{-2}
フォト	ph	1 ph=1cd sr cm^{-2} =10^4lx
ガル	Gal	1 Gal =1cm s^{-2}=$10^{-2}ms^{-2}$
マクスウエル	Mx	1 Mx = 1G cm^2=10^{-8}Wb
ガウス	G	1 G =1Mx cm^{-2} =10^{-4}T
エルステッド(a)	Oe	1 Oe ≙ (10^3/4π)A m^{-1}

(a) ３元系のCGS単位系とSIでは直接比較できないため、等号「 ≙ 」は対応関係を示すものである。

表10．SIに属さないその他の単位の例

名称	記号	SI 単位で表される数値
キュリー	Ci	1 Ci=3.7×10^{10}Bq
レントゲン	R	1 R = 2.58×10^{-4}C/kg
ラド	rad	1 rad=1cGy=10^{-2}Gy
レム	rem	1 rem=1 cSv=10^{-2}Sv
ガンマ	γ	1 γ=1 nT=10^{-9}T
フェルミ		1 フェルミ=1 fm=10^{-15}m
メートル系カラット		1 メートル系カラット= 0.2 g = 2×10^{-4}kg
トル	Torr	1 Torr = (101 325/760) Pa
標準大気圧	atm	1 atm = 101 325 Pa
カロリー	cal	1 cal=4.1858J（「15℃」カロリー），4.1868J（「IT」カロリー），4.184J（「熱化学」カロリー）
ミクロン	μ	1 μ =1μm=10^{-6}m

（第8版，2006年）